COMPU-EYE: a high resolution computational compound eye

Woong-Bi Lee,[1] Hwanchol Jang,[1] Sangjun Park,[1] Yong Min Song,[2] and Heung-No Lee[1,*]

[1]*School of Information and Communications, Gwangju Institute of Science and Technology, Gwangju, 61005, South Korea*

[2]*Department of Electronics Engineering, Pusan National University, Busan, 46241, South Korea*

[*]*heungno@gist.ac.kr*

Abstract: In nature, the compound eyes of arthropods have evolved towards a wide field of view (FOV), infinite depth of field and fast motion detection. However, compound eyes have inferior resolution when compared with the camera-type eyes of vertebrates, owing to inherent structural constraints such as the optical performance and the number of ommatidia. For resolution improvements, in this paper, we propose COMPUtational compound EYE (COMPU-EYE), a new design that increases acceptance angles and uses a modern digital signal processing (DSP) technique. We demonstrate that the proposed COMPU-EYE provides at least a four-fold improvement in resolution.

OCIS codes: (110.1758) Computational imaging; (100.6640) Superresolution; (110.3010) Image reconstruction techniques; (120.4570) Optical design of instruments.

References and links

1. E. Warrant and D.-E. Nilson, *Invertebrate Vision*, (Cambridge University, 2006), Chap. 1.
2. R. Dudley, *The Biomechanics of Insect Flight:Form, Function, Evolution*, (Princeton University, 2000), Chap. 5.
3. D. Floreano, J.-C. Zufferey, M. V. Scrinivasan, and C. Ellington, *Flying Insects and Robot*, (Springer, 2009), Chap. 10.
4. M. F. Land and D.-E. Nilson, *Animal Eyes* (Oxford University, 2002).
5. M. F. Land, "The optics of animal eyes," Contemp. Phys. **29**(5), 435–455 (1988).
6. D.-E. Nilson, "Vision optics and evolution," Bioscience **39**(5), 298–307 (1989).
7. A. Borst and J. Plett, "Optical devices: Seeing the world through an insect's eyes," Nature **497**(7447), 47–48 (2013).
8. Y. M. Song, Y. Xie, V. Malyarchuk, J. Xiao, I. Jung, K. J. Choi, Z. Liu, H. Park, C. Lu, R. H. Kim, R. Li, K. B. Crozier, Y. Huang, and J. A. Rogers, "Digital cameras with designs inspired by the arthropod eye," Nature **497**(7447), 95–99 (2013).
9. A. Brückner, J. Duparré, A. Bräuer, and A. Tünnermann, "Artificial compound eye applying hyperacuity," Opt. Express **14**(25), 12076–12084 (2006).
10. J. Duparré, F. Wippermann, P. Dannberg, and A. Bräuer, "Artificial compound eye zoom camera," Bioinspir. Biomim. **3**(4), 046008 (2008).
11. Y. Kitamura, R. Shogenji, K. Yamada, S. Miyatake, M. Miyamoto, T. Morimoto, Y. Masaki, N. Kondou, D. Miyazaki, J. Tanida, and Y. Ichioka, "Reconstruction of a High-Resolution Image on a Compound-Eye Image-Capturing System," Appl. Opt. **43**(8), 1719–1727 (2004).
12. K. H. Jeong, J. Kim, and L. P. Lee, "Biologically Inspired Artificial Compound Eyes," Science **312**(5773), 557–561 (2006).
13. D. P. Pulsifer, A. Lakhtakia, R. J. Martín-Palma, and C. G. Pantano, "Mass fabrication technique for polymeric replicas of arrays of insect corneas," Bioinspir. Biomim. **5**(3), 036001 (2010).
14. P. Qu, F. Chen, H. Liu, Q. Yang, J. Lu, J. Si, Y. Wang, and X. Hou, "A simple route to fabricate artificial compound eye structures," Opt. Express **20**(5), 5775–5782 (2012).
15. L. Li and A. Y. Yi, "Design and fabrication of a freeform microlens array for a compact large-field-of-view compound-eye camera," Appl. Opt. **51**(12), 1843–1852 (2012).
16. R. Hornsey, P. Thomas, W. Wong, S. Pepic, K. Yip, and R. Krishnasamy, "Electronic Compound-Eye Image Sensor: Construction and Calibration," Proc. SPIE **5301**, 13–24 (2004).
17. H. Zhang, L. Li, D. L. McCray, S. Scheiding, N. J. Naples, A. Gebhardt, S. Risse, R. Eberhardt, A. Tünnermann, and A. Y. Yi, "Development of a low cost high precision three-layer 3D artificial compound eye," Opt. Express **21**(19), 22232–22245 (2013).
18. D. Floreano, R. Pericet-Camara, S. Viollet, F. Ruffier, A. Brückner, R. Leitel, W. Buss, M. Menouni, F. Expert, R. Juston, M. K. Dobrzynski, G. L'Eplattenier, F. Recktenwald, H. A. Mallot, and N. Franceschini, "Miniature curved artificial compound eyes," Proc. Natl. Acad. Sci. U.S.A. **110**(23), 9267–9272 (2013).

#252751 Received 28 Oct 2015; revised 1 Jan 2016; accepted 10 Jan 2016; published 26 Jan 2016

19. T. Someya, T. *Stretchable Electronic*s (Wiley, 2013).
20. F. Marefat, A. Partovi, and A. Mousavinia, "A Hemispherical Omni-directional Bio Inspired Optical Sensor," in *Proceedings of Iranian Conference on Electrical Engineering (ICEE)* (2012), pp. 668–672.
21. M. F. Land, "Visual Acuity in Insects," Annu. Rev. Entomol. **42**(1), 147–177 (1997).
22. H. B. Barlow, "The size of ommatidia in apposition eyes," J. Exp. Biol. **29**, 667–674 (1952).
23. F. Zettler and R. Weiler, *Neural Principles in Visions* (Springer, 1976), Chap. 2.9.
24. G. Cristóbal, L. Perrinet, and M. S. Keil, *Biologically Inspired Computer Vision: Fundamentals and Applications* (Wiley-VCH, 2015).
25. P. T. Gonzalez-Bellido, T. J. Wardill, and M. Juusola, "Compound eyes and retinal information processing in miniature dipteran species match their specific ecological demands," Proc. Natl. Acad. Sci. U.S.A. **108**(10), 4224–4229 (2011).
26. H. C. Ko, M. P. Stoykovich, J. Song, V. Malyarchuk, W. M. Choi, C.-J. Yu, J. B. Geddes 3rd, J. Xiao, S. Wang, Y. Huang, and J. A. Rogers, "A hemispherical electronic eye camera based on compressible silicon optoelectronics," Nature **454**(7205), 748–753 (2008).
27. J. Tanida, T. Kumagai, K. Yamada, S. Miyatake, K. Ishida, T. Morimoto, N. Kondou, D. Miyazaki, and Y. Ichioka, "Thin observation module by bound optics (TOMBO): concept and experimental verification," Appl. Opt. **40**(11), 1806–1813 (2001).
28. C. Shi and F. Xu, "Post-digital image processing based on microlens array," Proc. SPIE **92701K**, 9270 (2014).
29. E. Watson, R. Muse, and F. Blommel, "Aliasing and blurring in microscaned imagery," Proc. SPIE **1689**, 242–250 (1992).
30. J. Oliver, W.-B. Lee, and H.-N. Lee, "Filters with random transmittance for improving resolution in filter-array-based spectrometers," Opt. Express **21**(4), 3969–3989 (2013).
31. H. Jang, C. Yoon, E. Chung, W. Choi, and H.-N. Lee, "Holistic random encoding for imaging through multimode fibers," Opt. Express **23**(5), 6705–6721 (2015).
32. J. Fang, J. Li, Y. Shen, H. Li, and S. Li, "Super-Resolution Compressed Sensing: An Iterative Reweighted Algotirhm for Joint Parameter Learning and Sparse Signal Recovery," IEEE Signal Process. Lett. **21**(6), 761–765 (2014).
33. M. Elad, *Sparse and redundant representations: from theory to applications in signal and image processing*. (Springer, 2010).
34. E. J. Candès, "Compressive sampling," Proc. Int. Congr. Mathematicians **3**, 1433–1452 (2006).
35. E. J. Candès, J. Romberg, and T. Tao, "Robust uncertainty principles: Exact signal reconstruction from highly incomplete frequency information," IEEE Trans. Inf. Theory **52**(2), 489–509 (2006).
36. D. L. Donoho, "Compressed sensing," IEEE Trans. Inf. Theory **52**(4), 1289–1306 (2006).
37. E. J. Candès and T. Tao, "Near-optimal signal recovery from random projections: universal encoding strategies?" IEEE Trans. Inf. Theory **52**(12), 5406–5425 (2006).
38. M. Aharon, M. Elad, and A. Bruckstein, "K-SVD: an algorithm for designing overcomplete dictionaries for sparse representation," IEEE T. Signal Process. **54**(11), 4311–4322 (2006).
39. R. Baraniuk, "Compressive sensing," IEEE Signal Process. Mag. **24**(4), 118–121 (2007).
40. D. L. Donoho, M. Elad, and V. Temlyakov, "Stable recovery of sparse overcomplete representations in the presence of noise," IEEE Trans. Inf. Theory **52**(1), 6–18 (2006).
41. E. J. Candès, J. Romberg, and T. Tao, "Stable signal recovery from incomplete and inaccurate measurements," Commun. Pure Appl. Math. **59**(8), 1207–1223 (2006).
42. A. Tavakoli and A. Pourmohammad, "Image Denoising Based on Compressed Sensing," Int. J. Comp. Theory Eng. **4**, 266–269 (2012).
43. J. Yang and Y. Zhang, "Alternating direction algorithms for l_1-problems in compressive sensing," SIAM J. Sci. Comput. **33**(1), 250–278 (2011).
44. A. Beck and M. Teboulle, "A fast iterative shrinkage-thresholding algorithm for linear inverse problems," SIAM J. Imaging Sci. **2**(1), 183–202 (2009).
45. A. Chambolle and T. Pock, "A first-order primal-dual algorithm for convex problems with applications to imaging," J. Math. Imaging Vis. **40**(1), 120–145 (2011).
46. W. Wang, M. J. Wainwright, and K. Ramchandran, "Information-theoretic limits on sparse signal recovery: Dense versus sparse measurement matrices," IEEE Trans. Inf. Theory **56**(6), 2969–2979 (2008).
47. E. J. Candès, Y. C. Eldar, D. Needell, and P. Randall, "Compressed sensing with coherent and redundant dictionaries," Appl. Comput. Harmon. Anal. **31**(1), 59–73 (2011).
48. H. Rauhut, "Compressive sensing and structured random matrices," Theor. Found. Num. Meth. Sparse Recov. **9**, 1–92 (2010).
49. R. Chartrand, "Fast algorithms for nonconvex compressive sensing: MRI reconstruction from very few data," in IEEE International Symposium on Biomedical Imaging (IEEE, 2009), pp. 262–265.
50. S. Boyd, N. Parikh, E. Chu, B. Peleato, and J. Eckstein, "Distributed Optimization and Statistical Learning via the Alternating Direction Method of Multipliers," Found. Trends Mach. Learn. **3**(1), 1–122 (2010).

1. Introduction

Compound eyes of arthropods such as ants, flies and bugs have attracted extensive research interest due to their unique features such as wide field-of-view (FOV), high sensitivity to motion and infinite depth of field [1–3]. An apposition type of compound eye in nature consists of integrated optical units called ommatidia, each of which includes a light diffracting

#252751 Received 28 Oct 2015; revised 1 Jan 2016; accepted 10 Jan 2016; published 26 Jan 2016

facet lens, crystalline cone, wave guiding rhabdom and photoreceptor cell [4–6]. Each ommatidium arranged along a spherical surface senses incident light within a small range of angular acceptance. Implementations of optical devices inspired by natural compound eyes exhibit great potential in various fields such as surveillance cameras on micro aerial vehicles, high-speed motion detection, endoscopic medical tools, and image guided surgery [7,8].

For years, several attempts to develop artificial compound eyes have been based on microlenses and photodetectors to imitate imaging organs of a natural ommatidium. Because most optoelectronics technologies developed earlier were intrinsically based on a planar substrate, both devices were implemented on a plane [9–11]. Planar compound eyes had low design and fabrication complexity, but they incurred a limited FOV. Later, curved microlens arrays were developed and interfaced with conventional planar sensors [12–17], but these suffered from off-axis aberrations, crosstalk between adjacent ommatidia, or restricted FOV [18]. They also required optical relay devices for beam-steering, which are complicated to fabricate [15–17]. In recent years, with the advance of flexible optoelectronics [19], curvilinear structured compound eyes, which provide larger FOVs, have been developed [8,18,20]. A hemispherical omni-directional optical sensor was implemented by a circular central board and multiple modular sensor boards [20]. Another cylindrical compound eye was introduced by bending the planar ommatidial array along a concave substrate [18]. Song. *et al*. implemented a hemispherical compound eye by reformulating stretchable planar ommatidia into hemispherical ommatidia [8]. We note that the hemispherically structured compound eye developed in [8], which is most comparable to a natural compound eye is mainly considered in this paper.

It is well known that the vision of insects is far inferior to that of humans because of inherent structural constraints [21–23]. Generally, the resolution of any eye depends not only on its optical resolution but also on the number of the receptors. First, if the optics are free of defects, the resolution of any optical imaging system is determined by its diffraction limit. The resolution of a diffraction-limited imaging system is proportional to the size of its lens and inversely proportional to the wavelength of the observed light. Second, in apposition-type compound eyes, the basic sampling units are ommatidia rather than photoreceptors. In a diffraction-limited compound eye, in order to accommodate many separate ommatidia without crosstalk, the number of ommatidia is much smaller than that of photoreceptors in the retina of a human eye. In nature, the density of the photoreceptors in the human eye is about 25 times higher than the ommatidial density of the compound eye [24]. For a compound eye to achieve a resolution similar to that of a human eye, it requires a radius of about 6 m and millions of ommatidia with facet lenses as large as a pupil, which is impractical [21].

Artificial compound eyes that mimic the structure of natural compound eyes are also limited on their image resolutions. In the design of the compound eyes, the spatial resolution that the compound eye can resolve depends on the relation between the acceptance angle ($\Delta\varphi$) of the ommatidia and the interommatidial angle ($\Delta\phi$) between the optical axes of the neighboring ommatidia [21,25]. In nature, for most light-adapted diurnal animals, the acceptance angles of ommatidia approach the interommatidial angle, i.e., $\Delta\varphi \approx \Delta\phi$ [21], which achieves high spatial resolution by minimizing aliasing among neighboring ommatidia. For example, *Tenodera* has angles $\Delta\varphi = 0.7°$ and $\Delta\phi = 0.6°$, and *Calliphora* has angles $\Delta\varphi = 1.02°$ and $\Delta\phi = 1.5°$. Analogous to natural compound eyes, artificially developed compound eyes have been designed to have similar acceptance and interommatidial angles [8,18]. The acceptance and interommatidial angles have been chosen to be $\Delta\varphi = 9.7°$ and $\Delta\phi = 11°$, and $\Delta\varphi = 4.2°$ and $\Delta\phi = \sim 4.2°$ in the literature [8,18]. Compared to the human eye, the artificial compound eyes are fundamentally limited on the resolution and thus they are inappropriate for object recognition.

For improving the quality of the observed image, a scanning method was introduced by capturing the object image repeatedly with different angle of rotations in [8,26]. As a result, an image of 160 × 160 pixels was obtained only with 16 × 16 ommatidia by scanning the compound-eye camera and thus the actual resolution of the observed image was improved by

#252751 Received 28 Oct 2015; revised 1 Jan 2016; accepted 10 Jan 2016; published 26 Jan 2016

100 times [8]. However, the repeated image capturing with fine mechanical angle controls makes the scanning method inefficient. In [27], a compact imaging system called TOMBO (thin observation module by bound optics) was introduced, which consists of a multi-aperture imaging system and a post-signal processing. The TOMBO reconstructs the object image with high resolution from multiple low-resolution subimages by exploiting the relation between the object and the captured signals. Afterward, many techniques were proposed to improve the reconstruction performance of the TOMBO system [27,28]. However, the FOVs are limited because they are planar compound eyes.

In this paper, instead of enhancing the size and number of the ommatidia for improving the resolution, we propose a totally different imaging system, called COMPUtational compound EYE (COMPU-EYE), using a modern digital signal processing (DSP) technique. Conventional compound eyes are designed to have limited ommatidial acceptance angles to avoid aliasing. Thus, each ommatidium of the conventional compound eye observes an independent section of the object image. In contrast, the ommatidium of COMPU-EYE has larger acceptance angles. This increase in acceptance angle allows a single ommatidium to observe multiple pieces of information simultaneously. Because the multiple pieces of information in each observation interfere with each other, the observed image is distorted. We employ a DSP technique in COMPU-EYE to recover the object image from these observations. In the DSP, by utilizing the fact that one piece of information is observed by multiple ommatidia with different perspectives, COMPU-EYE improves the resolution of the object image.

For a classical resolution improvement technique, a microscan technique requires to capture multiple frames of a target with slightly displaced locations [29]. The sequences of frames are then integrated to form a high resolution image. In contrast, COMPU-EYE provides a high resolution image reconstruction with a single frame of the target with less number of samples. The high resolution reconstruction is achieved by solving an underdetermined linear system of equations as will be introduced in Eq. (1) in Section 2. As a fast emerging area in DSP, compressed sensing (CS) provides a sparse solution to the underdetermined system. Recently, there are other papers who studied CS with the intension of improving resolution in various areas such as spectroscopy [30], optical imaging [31], and direction of arrival estimation [32]. In this paper, we propose to design a compound eye with large ommatidial acceptance angles, which is appropriate for the framework of the CS-based super-resolution, and reconstruct the object with high resolution using the DSP technique.

This paper is organized as follows: In Section 2, the system model of the compound eye imaging system is described. In Section 3, we propose COMPU-EYE and describe how COMPU-EYE improves the resolution by comparison with the conventional compound eye, and Section 4 presents the experimental results. Section 5 concludes the paper.

2. System description

We consider the biologically inspired compound eyes of a hemispherical structure as seen in Fig. 1(a). Details of the optical design of the hemispherical compound eye is referred from [8]. Each ommatidium, a basic imaging unit can be implemented by a set of microlens, supporting posts connected to a base membrane and a photodetector. An array of microlenses and photodiodes are integrated in the planar layout and are transformed into a full hemispherical shape. Note that the ommatidium is based on a circular lattice because the microlens is hemispherical shape compared to the hexagonal lattice in compound eyes in nature [21]. Each ommatidium receives incident light within its acceptance angle defined by $\Delta\varphi$ and is separated by an interommatidial angle $\Delta\phi$ from each other. We note that the optical transfer function of an ommatidium can be modeled as a Gaussian function. For simplicity, we assumed that the optical transfer function is simplified by neglecting light whose relative light intensities are smaller than a certain value. Thus, each ommatidium is modeled to collect averaged optical signal from light incident within its acceptance angle, $\Delta\varphi$, as seen in Fig. 1(b). With the compound eye of the hemispherical structure, we now consider an imaging system with M ommatidia as seen in Fig. 1(c). The imaging system observes an object image

#252751 Received 28 Oct 2015; revised 1 Jan 2016; accepted 10 Jan 2016; published 26 Jan 2016

on the plane size of $U \times V$ mm, which is located L mm away from the compound eye. According to the acceptance angle and object image distance, the receptive field (i.e., visible area at the object plane) of a single ommatidium is determined. Each observation contributes to a single pixel that contains the intensity of the light collected from its corresponding receptive field. The final image is reconstructed by a set of these pixels.

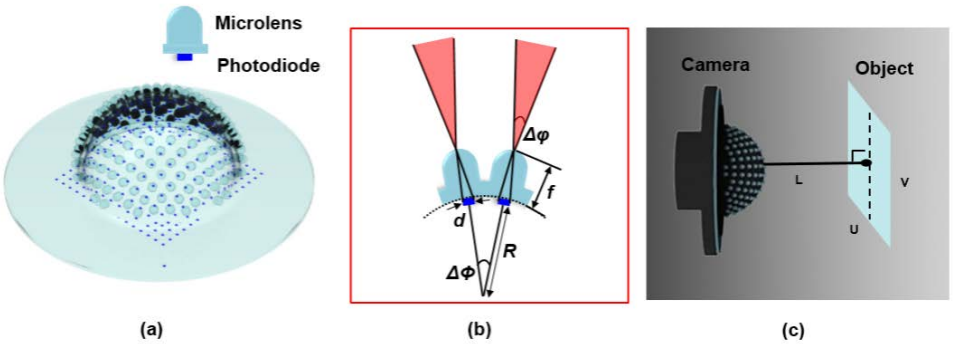

Fig. 1. (a) Illustration of the hemispherical compound eye. (b) Structure of conventional compound eye with key parameters: the acceptance angle ($\Delta\varphi$) and focal length (f) for each ommatidium, the interommatidial angle ($\Delta\phi$), the diameter of a photodiode (d) and the radius of curvature of the compound eye (R) and of an individual microlens (r). (c) Compound eye imaging system

Let y_i denote an output sample at the i^{th} ommatidium for $i \in \{1,2,\cdots,M\}$. We assume that the image to be reconstructed consists of N_U by N_V pixels, each having uniform light intensity. The size of each pixel is $U/N_U \times V/N_V$ mm. The object image forms an $N \times 1$ vector $\mathbf{x} = [x_1, x_2, \cdots, x_N]^T$, where $N = N_U N_V$. On the basis of ray tracing analysis, the sample y_i can be obtained from $y_i = \boldsymbol{a}_i \mathbf{x}$, where $\boldsymbol{a}_i$ is an $1 \times N$ vector whose elements represent the visibility of the i^{th} ommatidium at each of the N pixels. For the i^{th} ommatidium, if the j^{th} pixel for $j \in \{1,2,\cdots,N\}$ is outside the receptive field, which represents the j^{th} pixel is invisible to the i^{th} ommatidium, then the j^{th} component a_{ij} in $\boldsymbol{a}_i$ becomes zero, i.e., $a_{ij} = 0$. If the j^{th} pixel is inside the receptive field, which represents the j^{th} pixel is fully observed by the i^{th} ommatidium, then $a_{ij} = 1$. Otherwise, if the j^{th} pixel is on the boundary of the receptive field, which represents the j^{th} pixel is partially observed by the i^{th} ommatidium, then $0 < a_{ij} < 1$, which is proportional to the intersection area of the receptive field and pixel. This process can be summarized as follows:

$$a_{ij} = \begin{cases} 0 & , \ j^{\text{th}} \text{ pixel is invisible to } i^{\text{th}} \text{ ommatidium} \\ 1 & , \ j^{\text{th}} \text{ pixel is fully observed by } i^{\text{th}} \text{ ommatidium} \\ 0 < a_{ij} < 1, & j^{\text{th}} \text{ pixel is partially observed by } i^{\text{th}} \text{ ommatidium} \end{cases}.$$

When collecting M samples, the ommatidial observations can be modeled as a system of linear equations as follows:

$$\mathbf{y} = \mathbf{A}\mathbf{x} + \mathbf{n}. \tag{1}$$

where $\mathbf{y} = [y_1, \cdots, y_M]^T$ is a set of M output samples and $\mathbf{n} \in \mathbb{R}^{M \times 1}$ contains unexpected noise. Let $\mathbf{A} = [\boldsymbol{a}_1^T \ \boldsymbol{a}_2^T \cdots \boldsymbol{a}_M^T]^T \in \mathbb{R}^{M \times N}$ denote a measurement matrix the i^{th} row of which is $\boldsymbol{a}_i$. Given

#252751 Received 28 Oct 2015; revised 1 Jan 2016; accepted 10 Jan 2016; published 26 Jan 2016

the measurement matrix **A** and the observation **y**, we aim to solve the system of linear equations in Eq. (1) for the object image reconstruction.

In this paper, since we are considering resolution improvements in the compound eye imaging system, the number of estimated pixels is set to be greater than the number of ommatidia. i.e., $N > M$. Thereby, we note that Eq. (1) becomes an underdetermined system of linear equations. This underdetermined system can be solved by a convex optimization if the object is represented as a sparse signal in the proper domain [33–36]. A sparse signal is often represented as a vector which has a small number of non-zero components. We note that any natural image can be sparsely represented in a certain domain such as wavelets, the discrete cosine transform (DCT), or the discrete Fourier transform [37,38].

In an underdetermined system, the solution can be found by solving the l_0 minimization problem

$$\hat{\mathbf{x}} = \arg\min_{\mathbf{x}} \|\mathbf{x}\|_0 \quad \text{subject to} \|\mathbf{A}\mathbf{x} - \mathbf{y}\|_2 \le \varepsilon. \tag{2}$$

where $\|\mathbf{x}\|_0$ denotes the number of non-zero components in **x** and ε is a small positive constant. However, the optimization problem in Eq. (2) is combinatorial and computationally intractable [39]. Alternatively, the l_1 norm minimization provides unique and sparse solutions for underdetermined systems by solving

$$\hat{\mathbf{x}} = \arg\min_{\mathbf{x}} \|\mathbf{x}\|_1 \quad \text{subject to} \|\mathbf{A}\mathbf{x} - \mathbf{y}\|_2 \le \varepsilon. \tag{3}$$

We note that the l_1 norm minimization guarantees stability, which means that it can reliably reconstruct the signal without amplifying the observation errors in the process of l_1 norm minimization [40,41]. The l_1 norm minimization reconstructs a signal with explicit sparsity constraints while removing non-sparse random noise components from a corrupted signal. Due to its property of noise suppression, the l_1 norm minimization has been used as an image denoising tool [42]. Recently, many algorithms [43–45] have been proposed to solve Eq. (3). In this study, we use the alternating direction method [43], which is known to be fast and efficient for the problem in Eq. (3). If an object image of N pixels is reconstructed, where $N > M$, the resolution of COMPU-EYE is improved by a factor of N/M.

In the following section, we propose a COMPU-EYE imaging system, which is more appropriate to resolve Eq. (3) and thus to reconstruct the object image with high resolution.

3. COMPU-EYE for image acquisition and reconstruction with high resolution

In this section, we introduce COMPU-EYE. In COMPU-EYE, we propose to increase the acceptance angles of ommatidia larger than the interommatidial angle to recover the object image with computations. We first compare COMPU-EYE with the conventional compound eye imaging system in terms of resolution limit. We then explain how COMPU-EYE improves the resolution by investigating the influence of larger acceptance angles on the measurement matrix of the image capturing system.

#252751 Received 28 Oct 2015; revised 1 Jan 2016; accepted 10 Jan 2016; published 26 Jan 2016

3.1 Overview and comparison of compound eyes

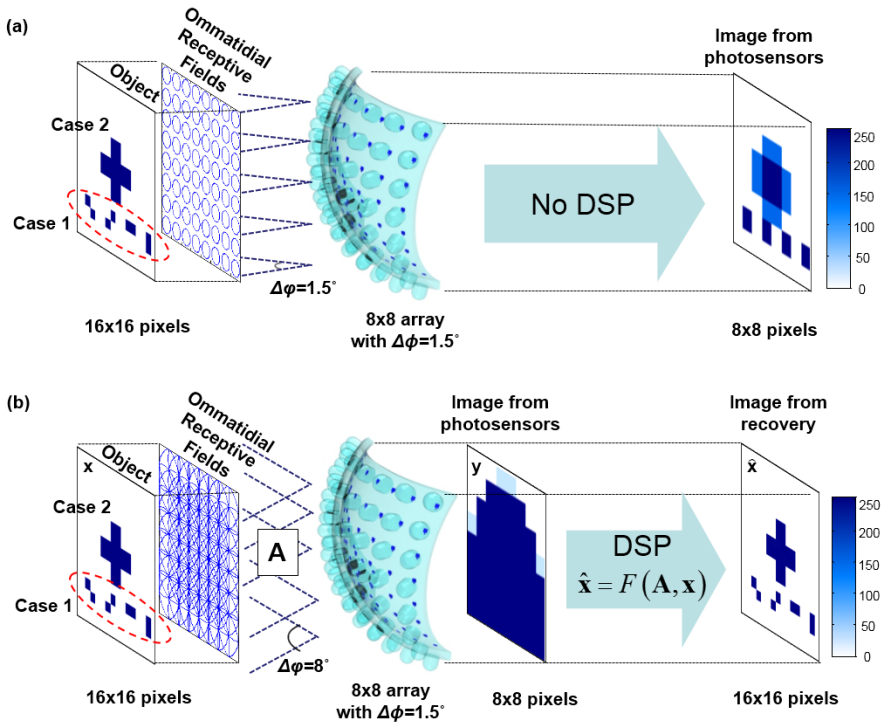

Fig. 2. Imaging systems of a conventional compound eye and the proposed COMPU-EYE (a) The conventional compound eye consists of 8 × 8 ommatidia with $\Delta\phi$ = 1.5° and $\Delta\varphi$ = 1.5°. (b) COMPU-EYE consists of 8 × 8 ommatidia with $\Delta\phi$ = 1.5° and $\Delta\varphi$ = 8° as well as a DSP algorithm.

The imaging system of a conventional compound eye is depicted in Fig. 2(a). It has a hemispherical structure with a radius (R) of 6.9216 mm, and consists of 8 × 8 ommatidia, each of which has a height (f) of 1.35 mm. Because each ommatidium provides a single sample, the compound eye has M = 64 samples. An 8 × 8 mm object image is located at a distance of 30 mm from the compound eye. The receptive field of a single ommatidium is shown as an ellipse, and a set of these receptive fields forms the ommatidial receptive fields near the left in Fig. 2(a).

In the conventional compound eye, the acceptance angles of the ommatidia are typically designed to be similar to the interommatidial angle (i.e., $\Delta\varphi = \Delta\phi = 1.5°$) in order to maximize the spatial resolution as well as to avoid overlapping ommatidial receptive fields. Accordingly, the ommatidial receptive fields are totally isolated, and each ommatidium observes an independent part of the object image. Each observation forms a single pixel in the reconstructed image. Note that no signal processing technique is needed to reconstruct the image.

To demonstrate the resolution limit of the conventional compound eye, we consider an object image comprising two parts as seen in Fig. 2(a): 1) four different patterns with the same light intensity, each of which is included in the receptive field of an ommatidium; and 2) a cross pattern that lies over several receptive fields.

Because every pattern in Case 1 is included within a receptive field, every observation appears to have a single image pixel with the same intensity of light. As a result, finer details within a receptive field cannot be resolved and the four different patterns in Case 1 cannot be distinguished by a conventional compound eye. Moreover, because its ommatidial receptive

#252751 Received 28 Oct 2015; revised 1 Jan 2016; accepted 10 Jan 2016; published 26 Jan 2016

fields are totally isolated, the fields contain *undetectable areas*, i.e., areas that are invisible to the compound eye. The undetectable areas deteriorate the image quality by decreasing the intensity of light observations as seen in right side of Fig. 2(a). This example shows that the conventional compound eye roughly recognizes object patterns, but has undetectable areas. As a result, such compound eyes suffer from limited resolution and poor image quality.

In contrast, consider the proposed COMPU-EYE imaging system in Fig. 2(b). COMPU-EYE consists of an 8 × 8 hemispherical array of ommatidia with acceptance angles that are larger than the interommatidial angle, i.e., $\Delta\varphi = 8° > \Delta\phi = 1.5°$. It is also equipped with a DSP technique. Because of the increased acceptance angles, the receptive field of each ommatidium is increased to at least 28 times that of $\Delta\varphi = 1.5°$. Thus, the ommatidial receptive fields widely overlap, severely distorting the observations as seen in the third frame from left in Fig. 2(b). We then apply DSP to recover a high resolution object image from these highly distorted observations.

In Fig. 2(b), the proposed COMPU-EYE recovers an object image of 256 pixels from 64 observations. The resolution is improved by a factor of four. In recovered image $\hat{\mathbf{x}}$, finer details that were perceived as a single point in Fig. 2(a) can be resolved, and different patterns in Case 1 are distinguished by COMPU-EYE. Moreover, COMPU-EYE compensates for undetectable areas and hence prevents the deterioration of the recovered image quality in Case 2. As a result, COMPU-EYE provides a higher-resolution image of better quality than the conventional compound eye.

3.2 Effects of larger acceptance angles and resolution improvements

We now focus on how larger acceptance angles along with the DSP technique improve resolution with respect to measurement matrix characteristics of the conventional compound eye and COMPU-EYE.

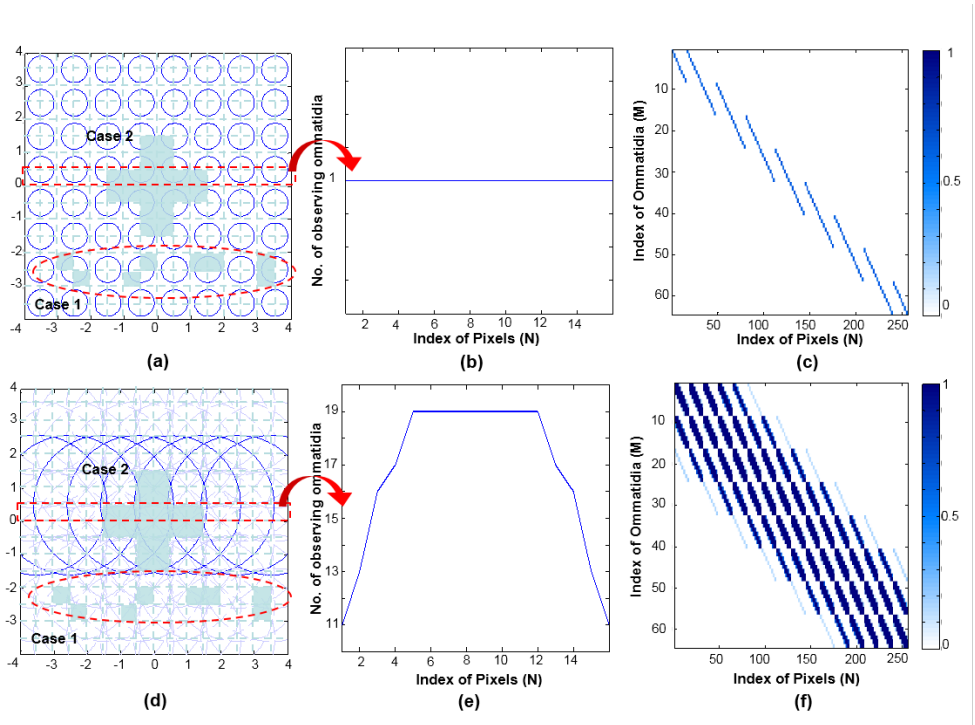

Fig. 3. Effects of acceptance angles for the conventional compound eye (top row) and COMPU-EYE (bottom row) (a)(d) Ommatidial receptive fields overlapped with the object image. (b)(e) Number of observing ommatidia corresponding to pixels in the 8th row. (c)(f) Graphical representations of the measurement matrices.

#252751 Received 28 Oct 2015; revised 1 Jan 2016; accepted 10 Jan 2016; published 26 Jan 2016

Figure 3(a) shows how the object image of a 16 × 16 array of pixels is projected onto the 8 × 8 ommatidial receptive fields of the conventional compound eye, where $\Delta\varphi = \Delta\phi = 1.5°$. The measurement matrix of the conventional compound eye $\mathbf{A} \in \mathbb{R}^{M\times N}$ in Eq. (1) can be obtained from the ommatidial receptive fields and pixels of the object image in Fig. 3(a). This measurement matrix is displayed graphically in Fig. 3(c). Every element in the measurement matrix indicates the visibility of the corresponding row of an ommatidium in the corresponding column of a pixel. Because the receptive fields of the ommatidia are small and isolated, the measurement matrix has few nonzero components. In Fig. 3(a), each ommatidium separately observes four corresponding pixels, and each pixel is observed by a single ommatidium. The values of the four pixels in one receptive field are considered to be of a single light intensity. Thus, each observation and its observed pixels are in a one-to-many correspondence relation. Because the information of one pixel is contained in one ommatidium as seen in Fig. 3(b), there is no additional information regarding that pixel in other observations. Therefore, in such relationships, finer details within the receptive field cannot be resolved and the resolution of the conventional compound eye is limited by M measurements. We note that the coefficients in Fig. 3(c) are smaller than one because the pixel cannot be entirely observed by ommatidia owing to the undetectable areas.

In contrast, COMPU-EYE has a larger acceptance angle of $\Delta\varphi = 8°$. Figure 3(d) shows how the object image is superimposed on the ommatidial receptive fields of COMPU-EYE. The size of each receptive field is considerably larger; a single ommatidium covers up to 76 pixels, which is considerably greater than the four pixels of the conventional compound eye. Whereas each receptive field in the conventional compound eye is small and separated, each receptive field in COMPU-EYE is large and highly overlapped. Hence, undetectable areas do not exist in the receptive fields of COMPU-EYE. As a result, the number of nonzero components increases correspondingly in the measurement matrix of COMPU-EYE in Fig. 3(f).

The measurement matrix of COMPU-EYE is appropriate for image acquisition and reconstruction rather than that of the conventional compound eye because the object elements, $\mathbf{x}$ in Eq. (1) is more likely to be aligned with the nonzero elements of the matrix [46]. As shown in Fig. 3(e), each pixel of the object image is observed multiple times with different ommatidia. In the context of information acquisition, the total quantity of information for a pixel is increased. Each observation is not redundant to the others for it has different receptive field. Accordingly, each column in the measurement matrix has multiple nonzero elements with different coefficients in Fig. 3(f). The observation of a pixel sufficiently differs from its other observations and this provides additional information about the pixel. In the literature, it is shown that such additional information is useful for reliable signal recovery, even if the number of measurements is smaller than the dimension of the original signal [31,37,46–48]. Thus, the large acceptance angle of ommatidia with the use of DSP allows COMPU-EYE to resolve finer details of the object beyond the resolution limit of M measurements.

#252751 Received 28 Oct 2015; revised 1 Jan 2016; accepted 10 Jan 2016; published 26 Jan 2016

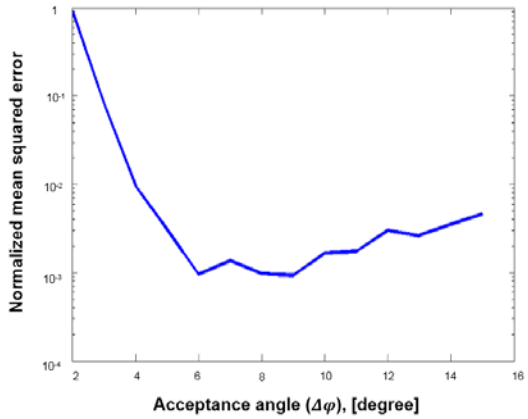

Fig. 4. NMSE against acceptance angle where $M = 8 \times 8$ ommatidia with $\Delta\phi = 1.5°$ and $N = 16 \times 16$ pixels.

We now investigate the reconstruction performance of the DSP technique in accordance with the acceptance angle in the example of Fig. 2. A randomly located sparse signal with 10 nonzero components is generated with uniform distribution between 0 and 1. As a measure of the reconstruction performance evaluation, let us define the normalized mean squared error (NMSE) as NMSE = $\|\hat{\mathbf{x}}-\mathbf{x}\|_2^2 / \|\mathbf{x}\|_2^2$. As seen in Fig. 4, when the acceptance angle is small, the object is unable to be reconstructed with low errors. Specifically, when $\Delta\phi = 2°$ which corresponds to the conventional compound eye in the example of Fig. 2(a), the 16×16 pixels cannot be recovered from 8×8 ommatidia. Associated with the measurement matrix in Fig. 3(c), each observation and its corresponding observed pixels are one-to-many correspondence. Thus, each ommatidium is unable to resolve fine details of its observation. As the acceptance angle increases, each pixel is observed multiple times by different ommatidia. The DSP technique reconstructs each pixel with low errors by solving Eq. (3). As a result, the NMSE decreases. When $\Delta\phi > 8°$, it is seen that the NMSE gradually increases because each observation becomes redundant with neighboring observations. We note that the analysis on the optimal acceptance angle is remained as our future works.

We note that the acceptance angle can be easily increased in many possible ways in an artificial compound eye. The acceptance angle within an ommatidium can be represented as $\Delta\varphi_o = \sqrt{(d/f)^2 + (\lambda/D)^2}$, where D is the lens diameter, λ is the light wavelength, d is the photosensor diameter, and f is the focal length of the ommatidial optics [21]. According to Snell's law, the acceptance angle $\Delta\varphi$ outside the ommatidium can be obtained by $\Delta\varphi = 2\sin^{-1}\left((n_0/n_1)\sin(\Delta\varphi_0/2)\right)$, where the refractive indices of the lens material and air are defined as n_0 and n_1, respectively. Thus, the acceptance angle $\Delta\varphi$ can be increased by using a material of higher refractive index for the ommatidia, decreasing the focal length f, or increasing the diameter d of the photodetector. Note that increasing the diameter of the photodetector may lead to increase the size of the ommatidia and the size of the compound eye. On the other hand, decreasing the radius of the curvature of the microlens for reducing the focal length can increase the acceptance angle without increasing the size of the ommatidia.

4. Results

To evaluate the performance of our design, we consider a hemispherical compound eye with a radius of $R = 6.9216$ mm, where each ommatidium has a height of $f = 1.35$ mm in Fig. 1(b). The compound eye consists of a varying number M of ommatidia of uniform spacing with the

#252751 Received 28 Oct 2015; revised 1 Jan 2016; accepted 10 Jan 2016; published 26 Jan 2016

interommatidial angle $\Delta\phi = 180/\sqrt{M}\,°$. The object image to be reconstructed is composed of $N = 160 \times 160$ pixels. As a sparsity measure of the image, we use the Sparsity Ratio (SR) defined as a ratio of the number of nonzero elements to the total length of the signal.

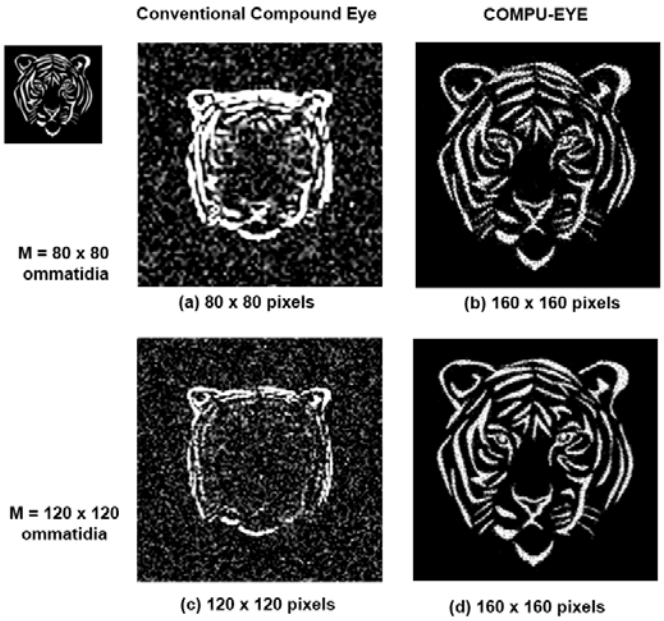

Fig. 5. For $M = 80 \times 80$ and $\Delta\phi = 2.25°$, (a) Output image of the conventional compound eye with $\Delta\varphi = 2.25°$ (b) Image recovered by COMPU-EYE with $\Delta\varphi = 60°$. For $M = 120 \times 120$ and $\Delta\phi = 1.5°$. (c) Output image of the conventional compound eye with $\Delta\varphi = 1.5°$ (d) Image recovered by COMPU-EYE with $\Delta\varphi = 60°$.

We demonstrate the performance of COMPU-EYE with an image in the presence of noise. The object image is a line-art illustration of a tiger, which consists of 160×160 pixels each of which contains an 8-bit quantized light intensity. The sparsity ratio of the tiger image is SR = 0.2335. The conventional compound eye consists of $M = 80 \times 80$ ommatidia with $\Delta\phi = \Delta\varphi = 2.25°$. On the other hand, COMPU-EYE consists of $M = 80 \times 80$ ommatidia of much larger acceptance angles, $\Delta\varphi = 60°$ than $\Delta\phi = 2.25°$. The object image size of 60×60 mm is at a distance of 10mm from the compound eyes. An additive observation noise in Eq. (1) is assumed to be Gaussian with zero mean and covariance matrix $\sigma^2\mathbf{I}_M$ where $\sigma^2 = 0.1$. Figure 5(a) shows the output image of the conventional compound eye. The output image is corrupted by noise. Because of the resolution limit determined by M and undetectable areas in the ommatidial receptive fields, the observed image of the conventional compound eye is poor quality. Figure 5(b) shows the image recovered by COMPU-EYE equipped with the DSP technique. Compared to the Fig. 5(a), COMPU-EYE provides a higher resolution imaging as well as denoising effects. Due to the stability of the l_1 norm minimization, the unexpected noise is efficiently removed in the reconstructed image without any denoising algorithm. When the number of ommatidia is increased to $M = 120 \times 120$ with $\Delta\phi = 1.5°$, the output image of the conventional compound eye and the recovered image of COMPU-EYE are shown in Figs. 5(c) and 5(d), respectively. As we increase the number of ommatidia, the object image is more clearly seen. For a measure of the resolution improvement, we define a *pixel resolution* as the total number of pixels to be reconstructed with NMSE $< \delta$, where $\delta > 0$ is a user-defined positive number. Since the number of pixels to be recovered is increased from 80^2 to 160^2 in Fig. 5(b) and from 120^2 to 160^2 in Fig. 5(d), the gain in the pixel

#252751 Received 28 Oct 2015; revised 1 Jan 2016; accepted 10 Jan 2016; published 26 Jan 2016

resolution is 4 and 1.78, respectively. We note that the size of the observed image in a conventional compound eye is smaller than that of the recovered image of the proposed eye; this is because the ommatidia on the edge of a conventional compound eye are unable to detect the object image owing to their small range of acceptance angle.

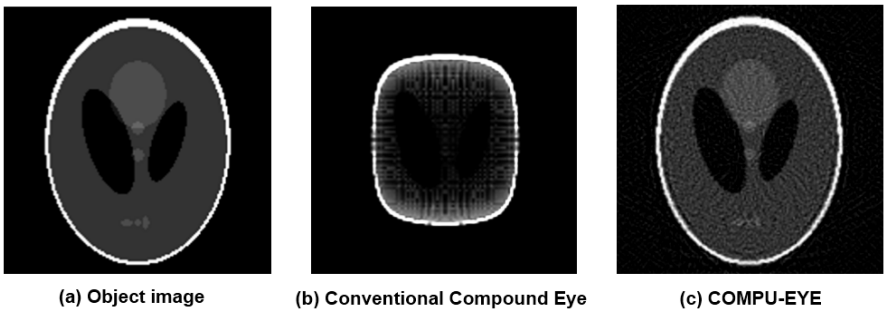

Fig. 6. For the compound eyes, M = 120 × 120 and $\Delta\phi$ = 1.5°. (a) Object image of 8-bit grayscale image with 160 × 160 pixels (b) Output image of the conventional compound eye with $\Delta\varphi$ = 1.5° and. (c) Image recovered by COMPU-EYE with $\Delta\varphi$ = 60°.

We now investigate the performance of COMPU-EYE with a non-sparse phantom image which is used in image processing [49]. The phantom image in Fig. 6(a) consists of 160 × 160 pixels, each of which contains an 8-bit intensity of light. SR of the phantom image is 0.4928. The number of ommatidia is set to be 120 × 120 with $\Delta\varphi$ = 1.5° and $\Delta\phi$ = 1.5° for the conventional compound eye and $\Delta\varphi$ = 60° and $\Delta\phi$ = 1.5° for COMPU-EYE. The object image size of 60 × 60 mm is at a distance of 10 mm from the compound eyes. In the reconstruction of the image, DCT is used for a sparsifying basis. As seen in Fig. 6(b), the direct observation of the conventional compound eye provides poor resolution and the object is distorted. Figure 6(c) shows the reconstructed image by COMPU-EYE. The resolution is improved by a factor of N/M = 1.78. We note that the distortion comes from a discrepancy in receptive fields of ommatidia, i.e., as an ommatidium is closely located to the edge of the compound eye, its corresponding receptive field becomes larger. In contrast, the reconstructed image of COMPU-EYE in Fig. 6(c) is not distorted because COMPU-EYE recovers the designated pixel values **x** in the object. As a result, COMPU-EYE can also reconstruct the non-sparse object image with a high resolution.

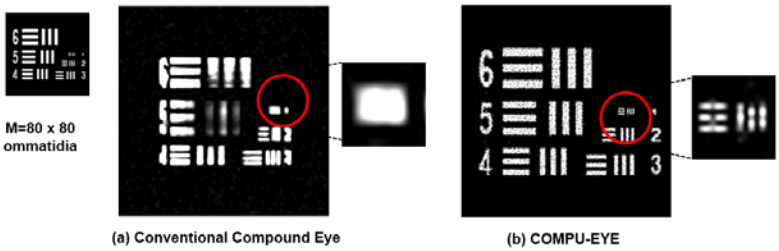

Fig. 7. Resolution test: (a) Conventional compound eye consisting of 80 × 80 ommatidia with $\Delta\varphi = \Delta\phi$ = 2.25°. (b) COMPU-EYE consisting of 80 × 80 ommatidia with $\Delta\varphi$ = 60° and $\Delta\phi$ = 2.25°.

Figure 7 illustrates optical resolution tests of the conventional compound eye and COMPU-EYE. The 60 × 60 mm object image at a distance of 10 mm is composed of 160 × 160 pixels. The object image is a target image similar to the US Air Force (USAF) test, where the minimum spacing of gratings is a single pixel, i.e., 0.375 mm. The lines of the row labeled

#252751 Received 28 Oct 2015; revised 1 Jan 2016; accepted 10 Jan 2016; published 26 Jan 2016

"1" have single pixel spacing, those of the row labeled "2" have two-pixel spacing, and so on. Both compound eyes are composed of 80 × 80 ommatidia with $\Delta\phi = 2.25°$ and $\Delta\varphi = 2.25°$ for the conventional compound eye and with $\Delta\phi = 2.25°$ and $\Delta\varphi = 60°$ for COMPU-EYE. Because the achievable optical resolution of the conventional 80 × 80 compound eye with $\Delta\varphi = \Delta\phi = 2.25°$ is 0.7179 × 0.7179 mm, which is obtained from the distance of resolvable gratings in the object plane, it cannot distinguish the smallest grating as shown in Fig. 7(a). However, COMPU-EYE can sharply resolve the smallest grating because the resolvable resolution is the unit of a single pixel. Thus, the achievable minimum optical resolution of COMPU-EYE is 0.375 × 0.375 mm, an improvement in resolution of about 3.66 times. We note that the observation at the center of the conventional compound eye in Fig. 7(a) suffers from lack of incoming light due to the relatively small sized receptive fields and its resulting undetectable area.

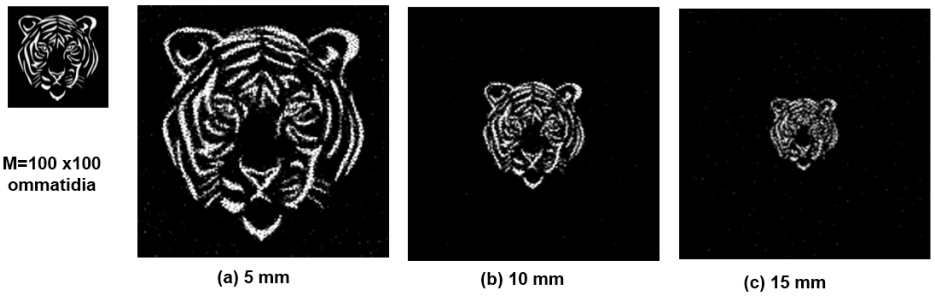

Fig. 8. Depth test: Image recovered by COMPU-EYE consisting of 100 × 100 ommatidia with $\Delta\varphi = 60°$ and $\Delta\phi = 1.8°$, where the dimension of the final object image is (a) 30 × 30 mm at 5 mm, (b) 60 × 60 mm at 10 mm, (c) 90 × 90 mm at 15 mm. The actual tiger picture is 30 × 30 mm.

Figure 8 shows the image recovered by the proposed COMPU-EYE at various object image distances. The size of the visible area of the compound eye is proportional to the distance of the object image, and the measurement matrices are generated according to the distances of the object image. Given the measurement matrices at distances of 5, 10, and 15 mm, the image can be reconstructed from **y**. As seen in Fig. 8, the recovered images are still clear and focus is maintained as the object image moves away from the compound eye.

5. Summary

In this study, we proposed the COMPU-EYE imaging system to improve the resolution of compound eyes. COMPU-EYE uses ommatidia with acceptance angles that are larger than the interommatidial angle as well as a DSP technique. By increasing the acceptance angles, each ommatidium covers wider areas, and each observation is different from the others because of its receptive field. Finer details can be resolved by the DSP technique. As a result, the proposed COMPU-EYE provides at least a four-fold improvement in resolution.

Natural compound eyes have the ability to detect high-speed motion owing to the simple ON/OFF detection structure of the ommatidium. In contrast, COMPU-EYE views the object only through computation and it necessarily requires certain computation time and cost for imaging. The computation requires solving a convex optimization problem; this problem can be solved in polynomial time by many state-of-the-art algorithms including YALL1 [43], FISTA [44], and CP [45]. Thus, the additional computation time required for the compound eyes is practically feasible with modern DSP devices. For example, when we measure the computation time using MATLAB with a 3.6-GHz Intel i7 processor, it takes 47 ms to recover $N = 256$ pixels from $M = 64$, as shown in Fig. 2(b). We note that the computation time can be reduced by using a multicore processor or graphic processing unit because the

#252751 Received 28 Oct 2015; revised 1 Jan 2016; accepted 10 Jan 2016; published 26 Jan 2016

algorithms [43–45] conduct matrix multiplications and additions, and these operations can be computed in parallel [50].

Generally, the acceptance angles are proportional to the light sensitivity of ommatidia. But, the large acceptance angles cause overlapping among neighboring ommatidia and necessarily result in low spatial resolution. By resolving the aliasing caused by the overlapping using a DSP technique, COMPU-EYE is expected to have high sensitivity with high resolution. Moreover, the technique for resolution improvements used in COMPU-EYE can be applied to other designs of artificial compound eyes. It would be interesting to compare resolution of Curvace design in [18] consisting of more ommatidia and the hemispherical compound eye in [8] consisting of less ommatidia but equipped with the DSP technique. In this paper, we have focused on the apposition compound eye. But, we note that the concept of COMPU-EYE can also be applied to other types of compound eyes, i.e., superposition compound eyes. For example, in the neural superposition compound eyes which are specialized for light sensitivity, each object point is imaged by multiple photoreceptors from different ommatidia and the related signals are combined to form an image with high sensitivity and high resolution [21]. By applying the design concept of larger acceptance angles and the DSP technique, the neural superposition compound eyes can improve the resolution and sensitivity. In the real implementation of compound eye devices, COMPU-EYE is more efficient in terms of multiple observations. If some ommatidia are disjointed or damaged, the conventional compound eye could lose vision in the corresponding area. However, in COMPU-EYE, each area is observed by multiple ommatidia. Thus, even though some ommatidia are lost, they do not have a significant influence on the overall observation.

Acknowledgments

This work was supported by the National Research Foundation of Korea (NRF) grant funded by the South Korean government (NRF-2015R1A2A1A05001826).

#252751 Received 28 Oct 2015; revised 1 Jan 2016; accepted 10 Jan 2016; published 26 Jan 2016